

# Biphasic Face Photo-Sketch Synthesis via Semantic-Driven Generative Adversarial Network with Graph Representation Learning

Xingqun Qi\*, Muyi Sun\*, Zijian Wang, Jiaming Liu, Qi Li, *Member, IEEE*, Fang Zhao, Shanghang Zhang, Caifeng Shan<sup>†</sup>, *Senior Member, IEEE*

**Abstract**—Biphasic face photo-sketch synthesis has significant practical value in wide-ranging fields such as digital entertainment and law enforcement. Previous approaches directly generate the photo-sketch in a global view, they always suffer from the low quality of sketches and complex photo variations, leading to unnatural and low-fidelity results. In this paper, we propose a novel Semantic-Driven Generative Adversarial Network to address the above issues, cooperating with Graph Representation Learning. Considering that human faces have distinct spatial structures, we first inject class-wise semantic layouts into the generator to provide style-based spatial information for synthesized face photos and sketches. Additionally, to enhance the authenticity of details in generated faces, we construct two types of representational graphs via semantic parsing maps upon input faces, dubbed the Intra-class Semantic Graph (IASG) and the Inter-class Structure Graph (IRSG). Specifically, the IASG effectively models the intra-class semantic correlations of each facial semantic component, thus producing realistic facial details. To preserve the generated faces being more structure-coordinated, the IRSG models inter-class structural relations among every facial component by graph representation learning. To further enhance the perceptual quality of synthesized images, we present a biphasic interactive cycle training strategy by fully taking advantage of the multi-level feature consistency between the photo and sketch. Extensive experiments demonstrate that our method outperforms the state-of-the-art competitors on the CUFS and CUFSF datasets.

**Index Terms**—Generative adversarial network, face photo-sketch synthesis, graph representation learning, intra-class and inter-class, iterative cycle training.

This work was supported by the Talent Introduction Program for Youth Innovation Teams of Shandong Province and also in part supported by the National Natural Science Foundation of China No.62306309.

Xingqun Qi is with the Academy of Interdisciplinary Studies, Hong Kong University of Science and Technology. (e-mail: xingqun.qi@connect.ust.hk).

Muyi Sun and Qi Li are with the CRIPAC, NLPR, Institute of Automation, Chinese Academy of Sciences, Beijing 100190, China. Muyi Sun is also with the School of Artificial Intelligence, Beijing University of Posts and Telecommunications, Beijing 100876, China (e-mail: muyi.sun@cripac.ia.ac.cn; qili@nlpr.ia.ac.cn).

Jiaming Liu and Shanghang Zhang are with the National Key Laboratory for Multimedia Information Processing, School of Computer Science, Peking University. (e-mail: jiamingliu@stu.pku.edu.cn, shanghang@pku.edu.cn).

Fang Zhao is with the School of Intelligence Science and Technology, Nanjing University, Nanjing 210023, China (e-mail: zhaofang0627@gmail.com).

Caifeng Shan is with the College of Electrical Engineering and Automation, Shandong University of Science and Technology, Qingdao 266590, China and also the School of Intelligence Science and Technology, Nanjing University, Nanjing 210023, China. (Email: caifeng.shan@gmail.com)

\* These authors contributed equally to this work. This work is done when Xingqun Qi was an intern at the CRIPAC, NLPR, Institute of Automation, Chinese Academy of Sciences, and also with the School of Computer Science, Peking University.

<sup>†</sup>Corresponding author: Caifeng Shan.

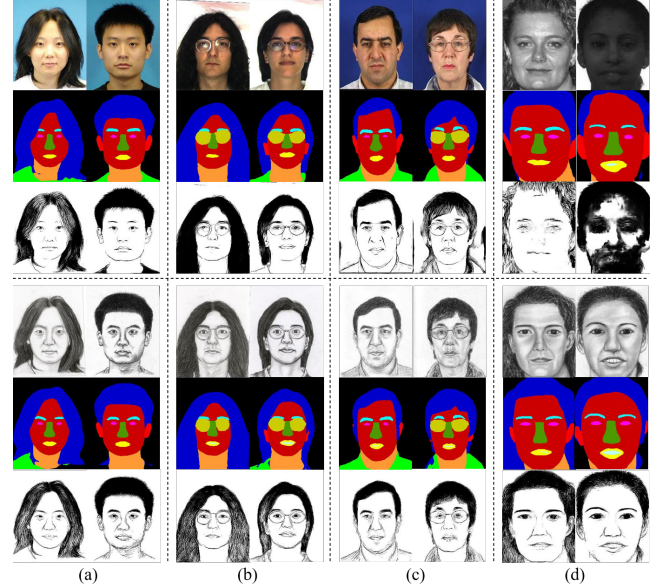


Fig. 1. Illustrations of samples with facial prior knowledge and parsing layout in different databases: (a) CUHK database, (b) AR database, (c) XM2VTS database, (d) CUFSF database. For each database, from top to bottom are face photos, the parsing layout of photos, the saliency detection result of photos, sketches, the parsing layout of sketches, and the saliency detection result of sketches, sequentially.

## I. INTRODUCTION

**B**IPHASIC face photo-sketch synthesis refers to generating sketches from face photos and, conversely, generating photos from face sketches. The wide-ranging application fields of the biphasic face photo-sketch synthesis include digital entertainment, law enforcement, and criminal case judgment. Specifically, face sketch is one of the most popular and fundamental portrait painting styles in the scope of digital entertainment [1]. In law enforcement and criminal case judgment, police commonly just hold the sketches of suspects drawn from the description of the witnesses. Face photos synthesized from these sketches with clear identities and manifest features can provide a feasible way to promote the efficiency of justice criminal cases [2]. However, it requires a vast time and effort to create distinct face sketches by professional artists. Due to the vital practical value, it is especially essential to automatically synthesize face photos and sketches with realistic effects and consistent identity preservation.

Numerous approaches have been proposed to address this task, which can be roughly grouped into exemplar-based approaches [3], linear-regression based approaches [4], and generative-model based ones [5]. Exemplar-based approaches [1], [3], [6]–[8] focus on bridging the mapping from photo to sketch via limited exemplar-paired patches, leading to over-smoothed and low personal identity results. Besides, linear-regression based approaches [9]–[12] always directly construct the linear mapping between photos and sketches. Recently developed generative-based methods [14]–[20] show better performance compared with the other two types. However, although these methods could generate sketches or face photos automatically, they adopted a holistic manner for generation and overlook the local specificity of different facial regions. Therefore, the face directly generated by these methods might yield distortion and noises in detailed parts. Meanwhile, the fidelity of the image and the consistency of the face identity also need to be improved.

Motivated by the above studies, we propose a novel Semantic-Driven Generative Adversarial Network with Graph Representation Learning for biphasic face photo-sketch synthesis. Our model is built upon the key insight that the human face has obvious spatial structures that determine the fidelity and identity consistency of face images. Therefore, the structural information should be enhanced by incorporating external prior or learned by designing specific objectives during the training process. In this paper, we design three methods to incorporate and learn structural information: saliency detection based guidance, face semantic injection, and two graph-based training objectives.

The saliency detection guidance utilizes the face saliency map as prior input to our network. Thanks to the recently advanced face saliency detection technique [21], we first leverage a pre-trained saliency detector to obtain the saliency maps, which incorporate overall facial structural information by identifying the most conspicuous or prominent parts of face images. As displayed in Fig 1, it is worth noting that the saliency map is different from the corresponding target sketch since the sketch contains more personal styles and textures of the painter *e.g.*, the shadows and outlines.

Then, considering the generated results should be structure consistent with the input human face, we perform face semantic injection in the network. Specifically, we transform the class-wise semantic layouts into two modulation parameters and inject them into the network decoder to provide style-based spatial information. In this fashion, the facial structure is well-preserved as well as the person’s identity is effectively guaranteed during the generation<sup>1</sup>. Here, we utilize a superior face parser to extract accurate semantic layouts for both photo and sketch, as depicted in Fig. 1.

To ensure the details of generated results are authentic, we propose two training objectives, which employ two novel graph representations for measuring facial structured information, dubbed the **Intra-class Semantic Graph (IASG)** and the **Inter-class Structure Graph (IRSG)**. In particular, IASG

leverages the human face semantic layouts as guidance to model the intra-class correlation of each facial component represented by a graph node. Here, we calculate the graph node as the mean center and variance center of the corresponding facial components. Considering that different facial components always contain large-range pixel numbers, we present an adaptive re-weighting algorithm to balance the contribution of detailed facial parts. Then, intra-class correlation can be effectively expressed by the similarity between the mean center (or variance center) and each pixel in the corresponding facial component. By enforcing the generated fake IASG to be consistent with the target ones, the details in the synthesized images achieve high-fidelity effects.

As a complement, the IRSG aims to keep the generated face photo and sketch more structure-coordinated with targets, globally. IRSG models the inter-class relations among every facial component. Concretely, the inter-class relations are built by computing the affinity scores between every two different mean centers (and variance centers). Similar to IASG, we utilize the target IRSG to supervise the synthesized fake ones, thus producing the natural human faces.

Moreover, based on the observation that the paired photo-sketch shared many personal characters, we design a novel biphasic iterative cycle training strategy to improve the perceptual quality of synthesized images. Here, we first train two models of photo generation and sketch generation, respectively. Then, we exploit the pre-trained sketch generation model as a personal knowledge extractor to boost photo generation. Iteratively, the sketch generation model is improved with the help of a pre-trained photo personal knowledge extractor. In this fashion, our framework enables high-quality biphasic face photo-sketch synthesis through multi-stage iterations. Extensive experiments demonstrate that our method significantly outperforms various counterparts, displaying natural and realistic facial details.

The main contributions of this study are summarized as:

- We propose a novel Semantic-Driven Generative Adversarial Network with Graph Representation Learning for generating realistic photos and distinct sketches.
- We construct two types of representational graphs and design corresponding constraints to facilitate the preservation of the details and coordinate structures in generated face photos and sketches.
- We propose a novel biphasic iterative cycle training to improve the perceptual quality of the synthesized images by effectively taking advantage of the multi-level feature consistency between the photo and sketch.
- Extensive comparison experiments are conducted on CUFS and CUFSF datasets, showing our method obtains state-of-the-art performance.

Compared to our preliminary work in [22], the improvements and extensions are consulted in three-fold: 1) We propose a novel inter-class structure graph that facilitates the preservation of the details and personal identities in generated face photos and sketches; 2) A novel biphasic iterative cycle training strategy is proposed to improve the perceptual quality of synthesized images; 3) We conduct the extension experiments on both sketch synthesis and face photo

<sup>1</sup>This is essential in sketch-to-photo synthesis when facing the criminal case judgment.

synthesis tasks. Driven by the aforementioned improvements, our framework achieves superior performance on **biphasic** photo-sketch synthesis in a **unified** manner. This significantly facilitates the application community on digital entertainment and law enforcement.

## II. RELATED WORK

### A. Biphasic Face Photo-Sketch Synthesis

Biphasic face photo-sketch synthesis has developed rapidly in the last few decades. Massive works have been proposed to solve this problem, which includes two closely related subtasks: face sketch synthesis and face photo synthesis. Therefore, researchers often analyze and discuss these two subtasks in a unified manner.

Deep neural network based approaches are the mainstream routine of biphasic photo-sketch synthesis in recent years, which have gradually emerged with the boost of Generative Adversarial Networks. Ji *et al.* [16] employed multi-domain adversarial methods to construct a mapping from photo-domain to sketch-domain. Zhu *et al.* [19] borrowed knowledge from transfer learning and proposed a lightweight network supervised by a high-performance larger network. Zhang *et al.* [23] embedded the photo parsing priors and designed a parametric sigmoid activation function in GAN based framework to facilitate robust sketch synthesis. Recently, Yu *et al.* [20] decomposed the face parsing layouts into multiple compositions and encoded them into conditional GAN (cGAN) for biphasic face photo-sketch synthesis which achieved state-of-the-art performance. Moreover, Duan *et al.* [18] introduced the gradient-based self-attention mechanism to combine the global residual connection and local residual connection in the proposed network which achieved better results. Besides, Zhang *et al.* [24] designed a dual transfer strategy to promote the biphasic face photo-sketch synthesis. Lin *et al.* [25] proposed the feature injection module to preserve the identity of synthesized sketches and photos. However, the sketches and photos synthesized by these methods are short of realistic detailed depictions.

Inspired by previous works, we inject the Semantic information into the generator of our proposed network. However, our injection module is different from previous works which embedded the multi-level identity feature into the network. In contrast, we aim at providing class-wise style-based spatial supervision for synthesized face photos and sketches. Furthermore, the previous work [25] did not follow the common experiment setting which ignored the influence of background on the generated results.

### B. Paired Image-to-Image Style Transfer

Paired image-to-image style transfer tasks can be regarded as a combination of image-to-image translation tasks and style transfer tasks. The image-to-image translation is often formulated as pixel-wise image generation tasks applied with paired images like biphasic face photo-sketch synthesis. Isala *et al.* [26] proposed a cGAN architecture to solve the image-to-image translation task with paired input and output named Pix2Pix. Due to the eminent performance of the Pix2Pix on the

paired dataset, researchers have made numerous improvements based on Pix2Pix and applied them to a wide range of research fields [27], [28], [67], [68]. By combining Pix2Pix and residual blocks, Wang *et al.* [29] proposed a novel network architecture to generate high-resolution images named pix2pixHD. Moreover, Park *et al.* [30] introduced the semantic layouts as spatial supervision injected in the pix2pixHD for synthesizing photorealistic images. Motivated by previous research, we exploit cGAN like Pix2Pix as our backbone network.

The biphasic face photo-sketch synthesis task can be treated as an image style transfer task between realistic photos and vivid sketch portraits. Gatys *et al.* [31] successfully applied pre-trained CNNs to the image style transfer task. Furthermore, Ulyanov *et al.* [32], [33] optimized the style transfer process by manipulating the Batch Normalization (BN) layers and Instance Normalization (IN) layers. Dumoulin *et al.* [34] utilized a group of parameters to realize the transfer of various image styles. Consecutively, Huang *et al.* [35] proposed the adaptive instance normalization (AdaIN) layers which could perform arbitrary style transfer without training repeatedly. Recently, Park *et al.* [13] put forward the spatially-adaptive normalization (SPADE) layers that inject the image style from the semantic layouts to obtain photorealistic images. Motivated by the previous research, we inject the style-based statistic information into the network to generate images with more distinct characteristics.

### C. Graph Representation Learning

Graph representation learning plays a significant role in computer vision tasks which could encode each node represented by a low-dimensional dense embedding in the graph structure [36]. Perozzi *et al.* [37] effectively embedded information of nodes by randomly sampling the graph structure. Furthermore, Defferrard *et al.* [38] designed a novel pooling strategy to rearrange the nodes for preserving more useful information of graph. Li *et al.* [39] constructed the structural graph of actions to capture the high-order dependencies between successive skeletons in the proposed actional-structural graph convolution network for skeleton-based action recognition. Besides, Ren *et al.* [40] adopted the graph generator to build the connections among spatial parts and construct the feature graph of these nodes representation for biometrics. Yang *et al.* [41] utilized a novel graph representation specifically designed for sketches by bridging the structural hierarchical relationship of sketches. This work has significantly improved the recognition accuracy of sketches. Wu *et al.* [65] propose an adaptive graph representation learning scheme for video person Re-ID, which enables the contextual interactions between relevant regional features. Jin *et al.* [66] introduce a self-supervised approach to learning graph node representations by enhancing Siamese self-distillation with multi-scale graph representation learning. As for the biphasic face photo-sketch synthesis task, Zhu *et al.* [7] combined graphical exemplar-based features with deep neural networks to synthesize high-quality sketches. The results synthesized by [7] are robust against lighting variations and clutter backgrounds. However, they still suffer from over-smoothing and



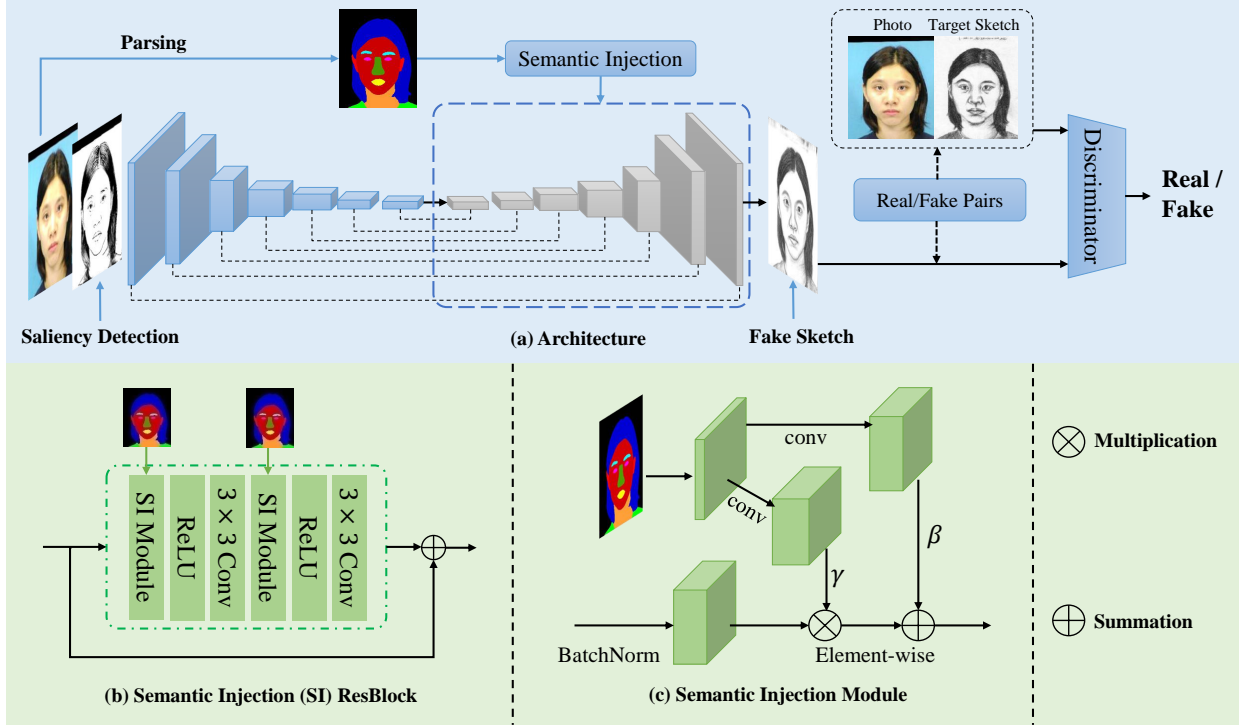


Fig. 2. The pipeline of our semantic-driven network. (a) The over architecture of the network exploits Pix2Pix as the backbone. The decoder contains several Semantic Injection (SI) ResBlocks with upsampling layers. (b) Details of Semantic Injection (SI) ResBlocks. (c) Details of Semantic Injection Module. In each Semantic Injection Module, the semantic map is convoluted to produce pixel-level normalization parameters  $\gamma$  and  $\beta$ .

lacking specific-identify characters in the synthesized photos and sketches. On the contrary, our graph representation learning algorithms can make restraint of intra-class features and inter-class features to help keep the realistic personal details of synthesized photos and sketches.

### III. METHOD

In this section, details about our proposed Semantic-Driven Generative Adversarial Network with Graph Representation Learning are presented. First, we introduce the preliminaries and problem formulation of our method. Afterward, the network architecture is described. Subsequently, we elaborate on the graph representation learning algorithms and biphasic iterative cycle training strategy. Finally, the objective functions of our model are introduced.

#### A. Preliminaries

Our semantic-driven network aims to construct a biphasic mapping of paired photo-sketch by utilizing class-wise semantic layouts as guidance. Previous researchers directly synthesize sketches or photos in a holistic manner, leading to unnatural and low-fidelity details in results. Our key insight is based on the observation that the human face has a distinct spatial structure. Here, we leverage the class-wise semantic layouts to model this structure information via graph representation learning. Specifically, the **IntrA**-class **Semantic Graph** (IASG) and the **Inter**-class **Structure Graph** (IRSG) are customized designed. Moreover, we present a novel biphasic iterative cycle training strategy to enhance the perceptual

quality of the synthesized images. Besides, we conduct facial saliency detection on the input images to provide overall prior information on facial structure. For brevity, we take the sketch synthesis task as the prototype to introduce the details.

Given paired photo-sketch training samples  $\{(x_i, y_i) | x_i \in X, y_i \in Y\}_{i=1}^N$ , where  $x_i$  represents photo and  $y_i$  represents sketch. The purpose of face sketch synthesis is to construct a mapping from the source photo domain  $X$  to the target sketch domain  $Y$ . As illustrated in Fig. 1, we find that there are complex variations in the source domain, resulting in severe impacts on the identity and fidelity of the generated sketches as depicted in Fig. 7 (c), (d) and Fig. 8 (c), (d). Conversely, in the photo generation task, the low-quality sketches of the source domain would affect the clarity of the generated image. Advanced face saliency detectors effectively capture the global structure information of the input photos or sketches. Regarding this, we first utilize face saliency detection results as prior information to provide the global facial structure. We concatenate the saliency map  $M$  and the face photo as the input to the generator. Besides, we also employ the pre-trained face parser to acquire semantic layouts  $S$  as guidance. Then, we inject this semantic information into our network to produce the final synthesized result. Therefore, the overall mapping can be formulated as  $\{X, M, S\} \rightarrow Y$ .

#### B. Semantic Driven Network Architecture

Fig. 2 illustrates the overall architecture of our network. First, we concatenate the paired saliency map and face photo as input. Pix2Pix [32] is exploited as the backbone including

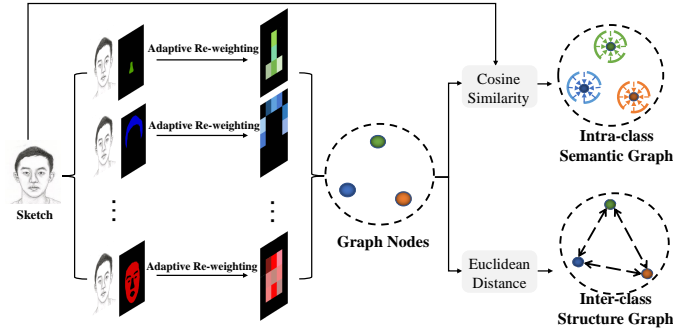


Fig. 3. Illustration of our proposed intra-class semantic graph and inter-class structure graph. The semantic masks are produced by a pre-trained face parsing network from the input photo. Besides, there are two types of graph nodes that represent the mean center and variance center of each facial component class.

7 convolutional and downsampling layers in the encoder part. Inspired by [36], we further design 7 Semantic Injection (SI) ResBlocks in the decoder to strengthen the conditional structure information guided by parsed semantic layouts. Each ResBlock contains two convolutional layers, two ReLU layers, and two Semantic Injection (SI) modules.

As shown in Fig. 2 (c), the SI module takes two inputs: the forward activation features after the Batch Normalization layer and semantic layouts obtained by pre-trained BiSeNet [42]. In order to prevent semantic ambiguity, we divide the human face into 12 spatial components: two eyes, two eyebrows, two ears, glasses, upper and lower lips, inner mouth, hair, nose, skin, neck, cloth, and background. Therefore, we have  $S = \{s^{(1)}, \dots, s^{(c)}\} \in \mathbb{R}^{h \times w \times c}$ , where  $c \in [1, 2, \dots, 12]$ ,  $s^{(c)} \in [0, 1]$ ,  $h$  and  $w$  denote the height and width of the semantic maps. Here, to inject the spatial structure information into the SI module, we perform the convolutional operation on semantic layouts. Thus, two modulation parameters  $\gamma$  and  $\beta$  are produced to normalize the final output. These two parameters encode sufficient spatial structure information. Then, we conduct multiplication and addition between these two modulation parameters and the normalized activation maps in an element-wise pattern as shown in Fig. 2 (c). In this fashion, the facial structure of the synthesized sketch is well-preserved with the input photo. Meanwhile, since the semantic layouts are robust to the complex variations of background, the generated sketches achieve the high-fidelity effect. Finally, we adopt a patch-wise discriminator to enforce the generated sketches keeping realism.

### C. Graph Representation Learning

Previously, researchers always impose global supervision on the entire generated sketches, resulting in defective performances in facial details. Thus, we construct two representational graphs named the **Intra-class Semantic Graph (IASG)** and the **Inter-class Structure Graph (IRSG)** to facilitate the preservation of the details in generated sketches as depicted in Fig. 3. Since different face components contain widely varying amounts of pixels, details in small components such as the two

eyes might be easily overlooked. Thus, to balance the contributions of different components, we treat each component as a graph node extracted in an adaptive re-weighting pattern.

1) *Intra-class Semantic Graph*: As illustrated in Fig. 3, the synthesized sketch is represented as  $F \in \mathbb{R}^{h_f \times w_f \times c_f}$ , where  $h_f$ ,  $w_f$  and  $c_f$  denote the height, width, and channel of the sketch, respectively. Here, we divide the synthesized sketch into 12 facial components guided by the aforementioned semantic layouts. Thus, each node of IASG is formulated as:

$$\mu(c) = \frac{1}{|S(:, :, c)|} \sum_{i=1}^{h_f} \sum_{j=1}^{w_f} S(i, j, c) F(i, j), \quad (1)$$

$$\nu(c) = \frac{1}{|S(:, :, c)|} \sum_{i=1}^{h_f} \sum_{j=1}^{w_f} \{S(i, j, c) F(i, j) - \mu(c)\}^2, \quad (2)$$

where  $|S(:, :, c)|$  represents the summation of pixel numbers in each facial component with the same semantic class  $c$ . Obviously, this strategy leverages the pixel number summation to normalize the contribution of each node, adaptive to different face components. Moreover,  $\mu(c)$  is considered as the mean center of all pixels in the  $c$ -th semantic category. Furthermore, the modulation variance  $\nu(c)$  can faithfully react to the semantic variation of the intra-class feature distribution. Note that both  $\mu$  and  $\nu$  are tensors in practice. As depicted in Fig. 3, each circle in the Graph Nodes represents different semantic classes by different colors. To model the intra-class correlation in each facial component, we calculate the cosine similarity between the synthesized sketch and each mean center (and variance center). Formally, the computation is listed as follows:

$$\begin{aligned} \mathbb{C}_1 &= \frac{F \cdot \mu}{\|F\|_2 \cdot \|\mu\|_2} \\ \mathbb{C}_2 &= \frac{F \cdot \nu}{\|F\|_2 \cdot \|\nu\|_2}. \end{aligned} \quad (3)$$

In this way, we construct the intra-class semantic graph for both the synthesized sketch and the target ones.

2) *Inter-class Structure Graph*: Subsequently, to ensure the generated sketch is structure-coordinated with the target, we model the inter-class structure relations among every two facial components in IRSG. Formally, the IRSG is expressed as:

$$\begin{aligned} \mathbb{G}_1 &= \langle \mu, \mathbb{E}_1 \rangle \\ \mathbb{G}_2 &= \langle \nu, \mathbb{E}_2 \rangle \end{aligned} \quad (4)$$

where the  $\mu$  and  $\nu$  represent nodes in the structure graph. Then, we utilize the edge  $\mathbb{E}$  between every two nodes to represent the structure relation of different facial components. Concretely, the graph edges are computed as the Euclidean Distance:

$$\begin{aligned} \mathbb{E}(c_1, c_2) &= \mathcal{E}(\mu(c_1), \mu(c_2)) \\ \mathbb{E}(c_1, c_2) &= \mathcal{E}(\nu(c_1), \nu(c_2)) \end{aligned} \quad (5)$$

where the  $c \in [1, 2, \dots, 12]$  denotes different facial components and  $\mathcal{E}$  represents the Euclidean Distance. Once we obtain the ITSG of both generated sketches and target ones, we exploit the target ITSG to constrain the synthesized sketches.

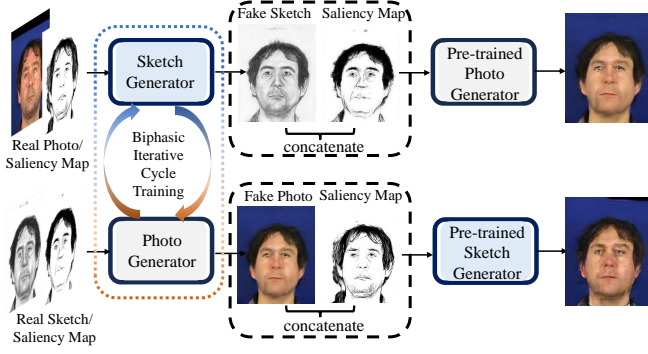


Fig. 4. The pipeline of our proposed iterative Training Strategy. The pre-trained photo generator is leveraged as a knowledge extractor to improve the perceptual quality of the generated fake sketch, iteratively.

#### D. Iterative Training Strategy

Inspired by the observation that paired photo-sketch shared personal characters, we propose a biphasic iterative cycle training strategy to improve the perceptual quality of the synthesized results as illustrated in Fig. 4. There are multi-stage in our iterative training strategy as reported in Algorithm 1. We name the generator and discriminator as  $G_k^i$ ,  $D_k^i$ ,  $G_o^i$  and  $D_o^i$ , where  $i \in \{0, 1, \dots, n\}$  denote the iterative stages;  $k$ ,  $o$  represent sketch synthesis and photo synthesis, respectively.

First, we train the generator and discriminator for the sketch synthesis task. Then, the photo generator and discriminator are trained similarly. Afterward, to improve the perceptual quality of generated sketch, we take the pre-trained photo generator as a knowledge extractor to boost the sketch generator and discriminator. Concretely, we take the generated fake sketch concatenated with saliency detection maps (produced from real sketch) feed into the pre-trained photo generator to acquire the fake photo. Then, we exploit the corresponding real sketch concatenated with saliency map feed into the photo generator to acquire the reconstructed photo. Then we leverage the reconstructed photo and corresponding feature maps to provide multi-scale supervision of the generated fake ones, thus significantly improving the sketch generator and discriminator. Once we obtain the updated sketch generation, we utilize it to enhance the performance of the photo generator and discriminator, iteratively. Note that this iterative cycle training strategy could be conducted on multi-stage until we obtain the optimal models.

#### E. Objective Function

The overall objective of our model includes following functions:  $\mathcal{L}_{GAN}$ ,  $\mathcal{L}_{content}$ ,  $\mathcal{L}_{IASG}$ ,  $\mathcal{L}_{perceptual}$ ,  $\mathcal{L}_{BCE}$ ,  $\mathcal{L}_{IRSG}$  and  $\mathcal{L}_{ICT}$ . Here, we adopt the sketch synthesis task as the prototype to elaborate the objective functions.

1) *Adversarial Loss.*: The adversarial loss is leveraged to correctly distinguish the real sketches or generated sketches. Similar to [32], the adversarial loss is formulated as:

$$\mathcal{L}_{GAN} = E_{X,M,Y} [\log D(X, M, Y)] + E_{X,M} [\log (1 - D(X, M, G(X, M)))], \quad (6)$$

#### Algorithm 1: The iterative training strategy of sketch synthesis

##### Input:

Input photo:  $X$ ; saliency detection map:  $M_o$ ; parsing mask:  $S_o$ ;  
Target sketch:  $Y$ ; saliency detection map:  $M_k$ ; parsing mask:  $S_k$ ;  
The number of iteration:  $i$ ; max iteration:  $T = 4$ ;

##### Output:

The optimal models  $G_k^i$  and  $D_k^i$ ;  
1 **Step1:** Initialize training  $G_k^0$ ,  $D_k^0$ ,  $G_o^0$  and  $D_o^0$ ;

2 **Step2:** Iterative training;

3 **for**  $i = 0$  **to**  $T$  **do**

4     Feed the  $X$ ,  $M_o$  and  $S_o$  to train the  $G_k^{i+1}$  and  $D_k^{i+1}$  which obtain fake sketch  $\hat{Y}$ ;

5     Feed the  $\hat{Y}$ ,  $M_k$  and  $S_k$  to the pre-trained  $G_o^i$  to obtain corresponding  $\hat{X}$ ; Extract multi-level feature maps from  $G_o^i$  as  $\hat{F}_o$ ;

6     Feed the  $Y$ ,  $M_k$  and  $S_k$  to the pre-trained  $G_o^i$  to obtain corresponding  $\tilde{X}$ ; Extract multi-level feature maps from  $G_o^i$  as  $F_o$ ;

7     Compute the loss between  $\hat{X}$  and  $\tilde{X}$ ,  $\hat{F}_o$  and  $F_o$ ;  
Back-propagate the gradients;

8 **end**

where  $X$ ,  $Y$  and  $M$  denote the source photos, target sketches and saliency detection maps.

2) *Content Loss.*: In addition, we utilize the normalized  $L_1$  distance to represent content loss.

$$\mathcal{L}_{content}(G) = E_{X,M,Y} [\|Y - G(X, M)\|_1]. \quad (7)$$

3) *Perceptual Loss.*: In order to ensure the generated sketch and the target sketch maintain similar specificity, we employ the pre-trained VGG-19 net [49] as a feature extractor to obtain high-level feature representations. We compare the features after the pool1 and pool2 layers.

$$\mathcal{L}_{perceptual} = \sum_{l=1}^2 \|\omega^l(Y) - \omega^l(G(X, M))\|_2^2, \quad (8)$$

where  $\omega^l(\cdot)$  represents the output feature maps and  $l$  denotes the selected pool1 and pool2 layers.

4) *Binary Cross-Entropy Parsing Loss.*: Moreover, we introduce the Binary Cross-Entropy (BCE) loss to further refine the synthesized sketch at the semantic level. We contrast the semantic mask of the synthesized sketch and the target sketch produced by the pre-trained parsing network [42].

$$\mathcal{L}_{BCE} = (\mathbb{P}(Y), \mathbb{P}(G(X, M))), \quad (9)$$

where  $\mathbb{P}$  denotes the inference process of parsing network.

5) *Intra-class Semantic Graph Loss.*: In practice, we extract the intra-class semantic graphs from the target sketch and synthesized sketch, respectively. Then, we reinforce the supervision of these intra-class semantic graphs to restrain the generated sketch from matching the feature distribution of the

target domain. The Intra-class Semantic Graph (IASG) loss is formulated:

$$\mathcal{L}_{IASG}(\mathbb{C}^{target}, \mathbb{C}^{fake}) = \sum_{r=1}^2 \sum_{c=1}^{12} \|\mathbb{C}_r^{target}(c) - \mathbb{C}_r^{fake}(c)\|_2^2, \quad (10)$$

where the  $r \in [1, 2]$  denotes two types of nodes of IASG represented by mean center and variance center.

6) *Inter-class Structure Graph Loss.*: Based on our preliminary work [22], we employ the Inter-class Structure Graphs (IRSG) to facilitate the coordinate structure preservation of synthesized sketches. Consequently, we apply the constraints between the IRSG of synthesized sketches and target sketches named IRSG Loss formulated as:

$$\mathcal{L}_{IRSG}(\mathbb{G}^{target}, \mathbb{G}^{fake}) = \sum_{r=1}^2 \sum_{c=1}^{12} \|\mathbb{G}_r^{target}(c) - \mathbb{G}_r^{fake}(c)\|_2^2. \quad (11)$$

where the  $r \in [1, 2]$  denotes two types of inter-class structure graphs with mean center and variance center.

7) *Iterative Cycle Training Loss.*: Finally, we design the Iterative Cycle Training (ICT) loss for the biphasic iterative training strategy. Four iterations are conducted in the experiments to reach the optimal results.

$$\mathcal{L}_{ICT} = \sum_{l=1}^5 \|G_o^{l,i}(Y) - G_o^{l,i}(G_k^i(X, M))\|_1, \quad (12)$$

where  $G_o^{l,i}(\cdot)$  denotes the photo generator and  $i$  represents the times of iteration. We select the feature maps to extract multi-level identity-specific information represented by  $l$ .

8) *Full Objective.*: Eventually, we combine all loss functions to achieve overall supervision:

$$\begin{aligned} \mathcal{L}_{total} = & \mathcal{L}_{GAN} + \alpha \mathcal{L}_{content} + \lambda \mathcal{L}_{perceptual} \\ & + \delta \mathcal{L}_{BCE} + \eta \mathcal{L}_{IASG} \\ & + \tau \mathcal{L}_{IRSG} + \xi \mathcal{L}_{ICT}. \end{aligned} \quad (13)$$

where the  $\alpha, \lambda, \delta, \eta, \tau$  and  $\xi$  are weighting factors. Furthermore, the generator  $G$  and the discriminator  $D$  could be optimized by the following formulation:

$$\min_G \max_D \mathcal{L}_{total} \quad (14)$$

#### IV. EXPERIMENTS

In this section, we first introduce the implementation details of our method. Then, we describe the datasets and evaluation criteria. Next, the experimental results are presented from both quantitative and qualitative perspectives, showing the effectiveness of our proposed method. Finally, we conduct the ablation study to verify each module.

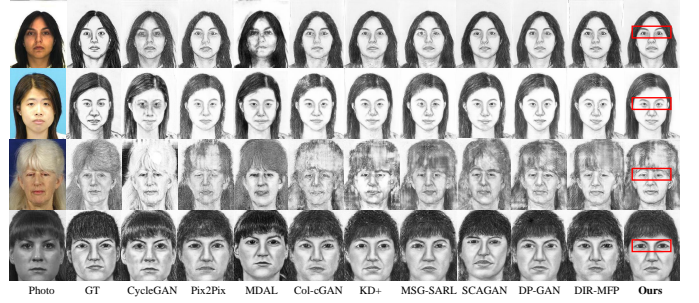


Fig. 5. Visualization of our generated sketches against various state-of-the-art methods, e.g. CycleGAN [59], Pix2Pix [26], MDAL [16], Col-cGAN [61], KD+ [19], MSG-SARL [18], SCAGAN [20], DP-GAN [62], DIR-MFP [63]. From top to bottom, samples of the first three rows are from the CUFS dataset, and the others are from the CUFSF dataset. Best view on screen.

#### A. Implementation Details

Both the generator and discriminator are implemented on the platform Pytorch [44] with a single NVIDIA GeForce Titan X GPU. We leverage the Adam optimizer with  $\beta_1 = 0.5$  and  $\beta_2 = 0.999$ . The total training epochs are 200, then the initial learning rate is set to 0.0002 for the first 100 epochs and decays linearly in the last 100 epochs. Additionally, we utilize the Instance Normalization [45], and set the batchsize = 1. Meanwhile, the weighting factors are set as  $\alpha = 100$ ,  $\lambda = 10$ ,  $\delta = 15$ ,  $\eta = 100$ ,  $\tau = 100$  and  $\xi = 5$ , respectively.

#### B. Datasets and Evaluation Criteria

We conduct extensive experiments on the CUHK Face Sketch Dataset (CUFS) [1] and the CUHK Face Sketch FERET Dataset (CUFSF) [46]. In the CUFS dataset, there are 606 faces, of which 188 faces are from the Chinese University of Hong Kong (CUHK) student database [3], 123 faces from the AR database [47], and 295 faces from the XM2VTS database [48]. For each sample, there are paired face photo-sketch drawn by the artist in natural lighting conditions. The CUFSF dataset contains 1194 face photos with paired sketches. However, all the photos in the CUFSF dataset are acquired under complex illumination variations as illustrated in Fig. 1 (d). For both datasets, we exploit the geometrical alignment strategy between the photos and sketches, based on the points of two eye centers and the mouth centers. Then, the aligned photo-sketch pair is cropped to  $200 \times 250$  following [49]. Meanwhile, we adopt the reshaping and padding conventions in [20] to expand the input image size to  $256 \times 256$ .

The experimental performance is measured by multiple metrics. We employ the Feature Similarity Index Metric (FSIM) [50] to evaluate the feature quality of synthesized sketches. FSIM is commonly utilized to measure the low-level similarity between the paired images, which extracts the phase congruence (PC) and the image gradient magnitude (GM) as features to index the quality. Consequently, blurring and noise of the generated images are evaluated by FSIM, ordinarily.

In addition, we apply the Structural Similarity Index Metric (SSIM) [51] to demonstrate the perceptual similarity between synthesized results and ground-truth images, which follows the visibility of humans. However, some works point out that



TABLE I

RESULTS ON FACE SKETCH SYNTHESIS IN THE CUFS AND THE CUFSF DATASETS.  $\uparrow$  INDICATES THE HIGHER IS BETTER,  $\downarrow$  INDICATES THE LOWER IS BETTER. OUR METHOD REACHES THE **OPTIMAL** AND **sub-optimal** RESULTS IN THE CUFS DATASET AND THE CUFSF DATASET.

	Model	CycleGAN	Pix2Pix	MDAL	KT	Col-cGAN	KD+	MSG-SARL	SCAGAN	DP-GAN	DIR-MFP	SDGAN	ours
CUFS	LPIPS(alex) $\downarrow$	0.2776	0.1654	-	0.2297	-	0.1971	-	-	-	-	0.1444	<b>0.1432</b>
	LPIPS(squeeze) $\downarrow$	0.1863	0.1156	-	0.1688	-	0.1471	-	-	-	-	0.1017	<b>0.0986</b>
	LPIPS(vgg-16) $\downarrow$	0.3815	0.3059	-	0.3483	-	0.3052	-	-	-	-	0.2767	<b>0.2646</b>
	FSIM $\uparrow$	0.6829	0.7356	0.7275	0.7373	-	0.7350	<b>0.7594</b>	0.716	0.7345	0.7378	0.7446	<b>0.7494</b>
	SSIM $\uparrow$	0.4638	0.5172	0.5280	-	0.5244	-	0.5288	-	-	<b>0.5703</b>	0.5360	<b>0.5493</b>
	FID $\downarrow$	58.394	44.272	-	-	-	-	46.39	34.2	-	-	33.408	<b>33.256</b>
CUFSF	LPIPS(alex) $\downarrow$	0.2234	0.1932	-	0.2522	-	0.2368	-	-	-	-	0.1906	<b>0.1867</b>
	LPIPS(squeeze) $\downarrow$	0.1617	0.1422	-	0.1740	-	0.1619	-	-	-	-	0.1370	<b>0.1341</b>
	LPIPS(vgg-16) $\downarrow$	0.3787	0.3551	-	0.3743	-	0.3550	-	-	-	-	0.3358	<b>0.3341</b>
	FSIM $\uparrow$	0.7011	0.7284	0.7076	0.7311	-	0.7171	0.7316	0.729	0.7080	0.7200	0.7328	<b>0.7332</b>
	SSIM $\uparrow$	0.3753	0.4204	0.3818	-	0.4224	-	0.4230	-	-	0.4215	0.4339	<b>0.4407</b>
	FID $\downarrow$	31.262	30.984	-	-	-	-	38.25	<b>18.2</b>	-	-	30.594	<b>24.577</b>

TABLE II

RESULTS ON FACE PHOTO SYNTHESIS IN THE CUFS AND CUFSF DATASETS.  $\uparrow$  INDICATES THE HIGHER IS BETTER,  $\downarrow$  INDICATES THE LOWER IS BETTER. OUR METHOD REACHES THE **OPTIMAL** AND **sub-optimal** RESULTS IN THE CUFS DATASET AND THE CUFSF DATASET. NOTE THAT THE RESULTS OF THE PS2MAN MODEL ARE DIRECTLY BORROWED FROM [19].

	Model	CycleGAN	Pix2Pix	KT	KD+	MSG-SARL	SCAGAN	PS2MAN	SDGAN	ours
CUFS	LPIPS(alex) $\downarrow$	0.2898	0.1687	0.1919	0.1717	-	-	0.2464	0.1674	<b>0.1497</b>
	LPIPS(squeeze) $\downarrow$	0.2509	0.1433	0.1747	0.1474	-	-	0.2158	0.1370	<b>0.1225</b>
	LPIPS(vgg-16) $\downarrow$	0.4383	0.3031	0.3208	0.2806	-	-	0.3254	0.2640	<b>0.2367</b>
	FSIM $\uparrow$	0.7270	0.7723	0.7851	0.7819	0.7866	0.795	0.7819	0.7845	<b>0.8001</b>
	SSIM $\uparrow$	0.4461	0.6086	-	-	0.6242	-	-	0.6543	<b>0.6822</b>
	FID $\downarrow$	124.540	86.996	-	-	66.17	<b>40.3</b>	-	63.937	<b>49.925</b>
CUFSF	LPIPS(alex) $\downarrow$	0.2271	0.2115	0.2440	0.2322	-	-	0.3145	0.2011	<b>0.1998</b>
	LPIPS(squeeze) $\downarrow$	0.1725	0.1669	0.2023	0.1791	-	-	0.2853	0.1581	<b>0.1556</b>
	LPIPS(vgg-16) $\downarrow$	0.3690	0.3579	0.3758	0.3565	-	-	0.4237	0.3422	<b>0.3376</b>
	FSIM $\uparrow$	0.7544	0.7855	0.7931	0.7789	0.7734	<b>0.845</b>	0.7812	0.7902	<b>0.7955</b>
	SSIM $\uparrow$	0.5594	0.6194	-	-	0.6114	-	-	0.6305	<b>0.6441</b>
	FID $\downarrow$	29.584	60.286	-	-	59.61	<b>20.6</b>	-	38.776	<b>38.372</b>

SSIM tends to favor over-smoothed images and ignores the texture of the results, which is not completely consistent with human perception [52]. Therefore, we introduce the Learned Perceptual Image Patch Similarity (LPIPS) [53] combined with SSIM to measure the perceptual visibility of synthesized results. LPIPS calculates the distance of embedding features between the generated images and target images. In this paper, LPIPS is exploited by three classification networks which are SqueezeNet [54], AlexNet [55], and VGGNet [43].

Besides, we adopt the Fréchet Inception Distance (FID) [56] to compute the Earth-mover distance (EMD) of distributions between the target domain and the synthesized image domain. Specifically, a pre-trained Inception-v3 network [57] is raised to measure the 2048-dimension features between the two contrast domains. FID is widely used in biphasic photo-sketch synthesis tasks and presents high confidence in image realism.

To evaluate the preservation of personal identity characteristics of the generated human faces, we introduce the face verification rate (FVR) which is implemented by Face++ API [58]. Previously, other researchers often use Null-space Linear Discriminant Analysis (NLDA) to measure identity-specific. However, NLDA is found to be seriously affected by image texture and deformations so it might not make an accurate assessment of identity-specific characteristics [19]. We utilize the Face++ APIs which the threshold is set as

73.975@FAR=1e-5 in our identity preservation experiments.

To demonstrate the superiority of our method, we adopt several benchmark approaches (*e.g.*, CycleGAN [59], Pix2Pix [26], MDAL [16], KT [60], Col-cGAN [61], KD+ [19], MSG-SARL [18], SCAGAN [20], DP-GAN [62], DIP-MFP [63] and PS2MAN [64]) for comparison. In addition, to further demonstrate the effectiveness of the proposed method, we also conduct comparison experiments between our preliminary work **SDGAN** [22] and our current model.

### C. Results on face sketch synthesis task

We verify the performance of our method on the face sketch synthesis on the CUFS and the CUFSF datasets. The experimental results are reported in Table I. Our method achieves the best capability on the indicators of LPIPS (alex), LPIPS (squeeze), LPIPS (vgg-16), and FID in the CUFS dataset. The proposed method decreases the previous best FID from 34.2 to 33.256. In addition, our method realizes the best performance on all indicators in the CUFSF dataset except FID. Obviously, the LPIPS (alex, squeeze, vgg) is significantly decreased with the large margin in both datasets which implies the higher fidelity and realism of the sketches generated by our method. In the sketch synthesis experiments, the MSG-SARL, DIR-MFP, and SCAGAN reach better results in limited metrics on the FSIM, SSIM, and FID. We observe



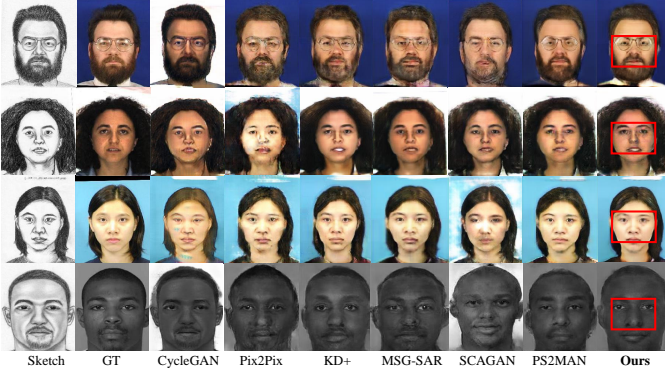


Fig. 6. Visualization of our generated photos against various state-of-the-art methods, *e.g.* CycleGAN [59], Pix2Pix [26], KD+ [19], MSG-SARL [18], SCAGAN [20], PS2MAN [64]. From top to bottom, samples of the first three rows are from the CUFS dataset, and the others are from the CUFSF dataset. Best view on screen.

that in Fig. 5, the generated images of these methods are more smoothed. Since the metrics such as SSIM is more kind to the smoothed image texture, this leads to better results than ours. However, we exploit the saliency map to provide global structure information. This results in better performance on the LPIPS and a more structural-coordinated human face.

We visualize the comparison of generated sketches among our method and various state-of-the-art counterparts as depicted in Fig. 5. Since the KT [5] is the preliminary conference version of KD+ [4], we only display the better version in the experiments. We observe that CycleGAN and MDAL produce low-fidelity sketches compared with ground truth. The results of Col-cGAN, MSG-SARL, and SCAGAN contain blur and noisy effects. Conversely, our method achieves the best performance, especially in the detailed facial components such as the eyes, ears, and hair contours (*e.g.*, in the red boxes of the last column).

#### D. Results on face photo synthesis task

Compared with face sketch synthesis, there are fewer previous methods that focus on the photo synthesis task. Our method obtains the best performance with LPIPS (alex, squeeze, vgg) and SSIM on both datasets. According to Table II, the SCAGAN [20] achieves better results than our method with FSIM and FID because of its stacking architecture. In contrast, our network is end-to-end that has stronger practical significance on edge devices. It is more challenging to synthesize photos from the CUFSF dataset. As shown in Fig. 1 (d), there are illumination variations in the CUFSF dataset. Meanwhile, all photos are grayscale and sketches are drawn with deformation.

We display the visual comparison in Fig. 6. Pix2Pix, MSG-SAR, and SCAGAN synthesize the natural photos compared with the ground truth faces. CycleGAN, KD+, and PS2MAN generate better results while their faces contain less stylized textures of the painter. On the contrary, our method achieves vivid and realistic photo synthesis. As highlighted in the red boxes, the facial structures of our results are much more natural than other competitors.

TABLE III  
COMPARISON BETWEEN THE PRELIMINARY WORK **SDGAN** AND OUR CURRENT NETWORK NAMED **OURS** IN THE TABLE ALL THE PERFORMANCES OF OUR CURRENT MODEL ARE **BETTER** THAN PRELIMINARY WORK.  $\uparrow$  INDICATES THE HIGHER IS BETTER,  $\downarrow$  INDICATES THE LOWER IS BETTER.

Task		Sketch Synthesis			Photo Synthesis		
Model		SDGAN	Ours	Gap	SDGAN	Ours	Gap
CUFS	LPLPS (alex) $\downarrow$	0.1444	<b>0.1432</b>	0.0012	0.1674	<b>0.1497</b>	0.0177
	LPIPS (squeeze) $\downarrow$	0.1017	<b>0.0986</b>	0.0031	0.1370	<b>0.1225</b>	0.0145
	LPIPS (vgg-16) $\downarrow$	0.2767	<b>0.2646</b>	0.0021	0.2640	<b>0.2367</b>	0.0273
	FSIM $\uparrow$	0.7446	<b>0.7494</b>	0.0048	0.7845	<b>0.8001</b>	0.0156
	SSIM $\uparrow$	0.5360	<b>0.5493</b>	0.0133	0.6543	<b>0.6822</b>	0.0279
	FID $\downarrow$	33.408	<b>33.256</b>	0.152	63.937	<b>49.925</b>	14.012
	FVR $\uparrow$	86.179	<b>87.542</b>	1.363	79.040	<b>81.780</b>	2.74
CUFSF	LPIPS (alex) $\downarrow$	0.1906	<b>0.1867</b>	0.0039	0.2011	<b>0.1998</b>	0.0013
	LPIPS (squeeze) $\downarrow$	0.1370	<b>0.1341</b>	0.0029	0.1581	<b>0.1556</b>	0.0025
	LPIPS (vgg-16) $\downarrow$	0.3358	<b>0.3341</b>	0.0017	0.3422	<b>0.3376</b>	0.0046
	FSIM $\uparrow$	0.7328	<b>0.7332</b>	0.0004	0.7902	<b>0.7955</b>	0.0053
	SSIM $\uparrow$	0.4339	<b>0.4407</b>	0.0068	0.6305	<b>0.6441</b>	0.0136
	FID $\downarrow$	30.594	<b>24.577</b>	6.017	38.776	<b>38.372</b>	0.404
	FVR $\uparrow$	86.758	<b>87.109</b>	0.351	62.763	<b>63.344</b>	0.581

#### E. Comparison with preliminary work

To evaluate the improvement between our current model and preliminary work **SDGAN**, we conduct the performance comparison as reported in Table III.

Since SDGAN supervises the synthesis of sketches and photos in the intra-class semantic space, the generated human faces always have abundant detailed features. However, SDGAN does not effectively extract the structure knowledge in the facial images, which is modeled by the inter-class structure graph in the current framework. Therefore, we take advantage of both intra-class semantic and inter-class structure graph representations that allow the synthesized human faces to be more clearly structured and contain distinctive features, as illustrated in columns (h-j) of Fig. 7 and columns (g-i) of Fig. 8. Besides, the SDGAN is designed for unidirectional photo-sketch synthesis that overlooks there are personal-identity consistency between the paired photo-sketch. On the contrary, with the help of the biphasic iterative cycle training strategy, the identity-preserving ability of our current model is significantly enhanced. This is essential in the image-to-image translation task with geometrical alignment datasets. As reported in Table IV and Table V, the Face verification Rate (FVR) significantly increased after applying the biphasic iterative cycle training strategy. Besides, as illustrated in Table III, our current model performance has been significantly raised compared with preliminary **SDGAN**, especially in the photo synthesis task. From a more intuitive point of view, the human faces synthesized by the current model give the expression of more fidelity and consistency than **SDGAN**.

TABLE IV

THE ABLATION STUDY ON CUFS DATASET.  $\uparrow$  INDICATES THE HIGHER IS BETTER,  $\downarrow$  INDICATES THE LOWER IS BETTER. NOTE THAT OUR PRELIMINARY WORK **SDGAN** IS INDICATED AS THE LAST **3rd** ROW FROM UP TO BOTTOM IN EACH TASK.

	Model Variations									Criterion						
	Backbone	Salicency Mask $M$	Parsing Layouts $S$	Perceptual Loss	BCE Loss	IASG Loss	IRSG Loss	ICT Loss		LPIPS (alex) $\downarrow$	LPIPS (squeeze) $\downarrow$	LPIPS (vgg-16) $\downarrow$	FSIM $\uparrow$	SSIM $\uparrow$	FID $\downarrow$	FVR $\uparrow$
Sketch Synthesis	$\checkmark$	-	-	-	-	-	-	-		0.1654	0.1156	0.3059	0.7356	0.5172	44.272	84.252
	$\checkmark$	$\checkmark$	-	-	-	-	-	-		0.1581	0.1141	0.3080	0.7376	0.5145	42.367	84.504
	$\checkmark$	$\checkmark$	$\checkmark$	-	-	-	-	-		0.1570	0.1108	0.2965	0.7411	0.5286	41.048	84.698
	$\checkmark$	$\checkmark$	$\checkmark$	$\checkmark$	-	-	-	-		0.1644	0.1123	0.2918	0.7424	0.5248	34.854	83.893
	$\checkmark$	$\checkmark$	$\checkmark$	$\checkmark$	$\checkmark$	-	-	-		0.1642	0.1138	0.2918	0.7433	0.5311	34.638	84.892
	$\checkmark$	$\checkmark$	$\checkmark$	$\checkmark$	$\checkmark$	$\checkmark$	-	-		0.1444	0.1017	0.2767	0.7446	0.5360	33.408	86.179
	$\checkmark$	$\checkmark$	$\checkmark$	$\checkmark$	$\checkmark$	$\checkmark$	$\checkmark$	-		0.1446	0.0995	0.2727	0.7466	0.5482	<b>33.166</b>	86.648
	$\checkmark$	$\checkmark$	$\checkmark$	$\checkmark$	$\checkmark$	$\checkmark$	$\checkmark$	$\checkmark$		<b>0.1432</b>	<b>0.0986</b>	<b>0.2646</b>	<b>0.7494</b>	<b>0.5493</b>	<b>33.256</b>	<b>87.542</b>
Photo Synthesis	$\checkmark$	-	-	-	-	-	-	-		0.1687	0.1433	0.3031	0.7723	0.6086	86.996	73.527
	$\checkmark$	$\checkmark$	-	-	-	-	-	-		0.1660	0.1449	0.3018	0.7742	0.6093	93.204	74.046
	$\checkmark$	$\checkmark$	$\checkmark$	-	-	-	-	-		0.1589	0.1341	0.2788	0.7759	0.6266	66.176	75.260
	$\checkmark$	$\checkmark$	$\checkmark$	$\checkmark$	-	-	-	-		0.1609	0.1341	0.2799	0.7777	0.6303	64.495	76.427
	$\checkmark$	$\checkmark$	$\checkmark$	$\checkmark$	$\checkmark$	-	-	-		0.1562	0.1326	0.2760	0.7788	0.6320	65.729	76.778
	$\checkmark$	$\checkmark$	$\checkmark$	$\checkmark$	$\checkmark$	$\checkmark$	-	-		0.1674	0.1370	0.2640	0.7845	0.6543	63.937	79.040
	$\checkmark$	$\checkmark$	$\checkmark$	$\checkmark$	$\checkmark$	$\checkmark$	$\checkmark$	-		0.1571	0.1306	0.2588	0.7892	0.6627	61.726	78.438
	$\checkmark$	$\checkmark$	$\checkmark$	$\checkmark$	$\checkmark$	$\checkmark$	$\checkmark$	$\checkmark$		<b>0.1497</b>	<b>0.1225</b>	<b>0.2367</b>	<b>0.8001</b>	<b>0.6822</b>	<b>49.925</b>	<b>81.780</b>

TABLE V

THE ABLATION STUDY ON CUFSF DATASET.  $\uparrow$  INDICATES THE HIGHER IS BETTER,  $\downarrow$  INDICATES THE LOWER IS BETTER. NOTE THAT OUR PRELIMINARY WORK **SDGAN** IS INDICATED AS THE LAST **3rd** ROW FROM UP TO BOTTOM IN EACH TASK.

	Model Variations									Criterion						
	Backbone	Salicency Mask $M$	Parsing Layouts $S$	Perceptual Loss	BCE Loss	IASG Loss	IRSG Loss	ICT Loss		LPIPS (alex) $\downarrow$	LPIPS (squeeze) $\downarrow$	LPIPS (vgg-16) $\downarrow$	FSIM $\uparrow$	SSIM $\uparrow$	FID $\downarrow$	FVR $\uparrow$
Sketch Synthesis	$\checkmark$	-	-	-	-	-	-	-		0.1932	0.1422	0.3551	0.7284	0.4204	30.984	86.027
	$\checkmark$	$\checkmark$	-	-	-	-	-	-		0.1939	0.1429	0.3562	0.7275	0.4193	29.765	85.772
	$\checkmark$	-	$\checkmark$	-	-	-	-	-		0.2037	0.1443	0.3454	0.7290	0.4297	30.970	86.052
	$\checkmark$	-	$\checkmark$	$\checkmark$	-	-	-	-		0.2070	0.1423	0.3545	0.7299	0.4270	28.639	86.099
	$\checkmark$	-	$\checkmark$	$\checkmark$	$\checkmark$	-	-	-		0.1983	0.1420	0.3460	0.7300	0.4282	25.723	86.512
	$\checkmark$	-	$\checkmark$	$\checkmark$	$\checkmark$	$\checkmark$	-	-		0.1906	0.1370	0.3358	0.7328	0.4339	30.594	86.758
	$\checkmark$	-	$\checkmark$	$\checkmark$	$\checkmark$	$\checkmark$	$\checkmark$	-		0.1896	0.1370	0.3349	0.7321	0.4355	28.995	87.023
	$\checkmark$	-	$\checkmark$	$\checkmark$	$\checkmark$	$\checkmark$	$\checkmark$	$\checkmark$		<b>0.1867</b>	<b>0.1341</b>	<b>0.3341</b>	<b>0.7332</b>	<b>0.4407</b>	<b>24.577</b>	<b>87.109</b>
Photo Synthesis	$\checkmark$	-	-	-	-	-	-	-		0.2115	0.1669	0.3579	0.7855	0.6194	60.286	62.074
	$\checkmark$	-	$\checkmark$	-	-	-	-	-		0.2137	0.1653	0.3546	0.7875	0.6243	42.517	61.322
	$\checkmark$	-	$\checkmark$	$\checkmark$	-	-	-	-		0.2106	0.1672	0.3537	0.7882	0.6219	51.397	62.174
	$\checkmark$	-	$\checkmark$	$\checkmark$	$\checkmark$	-	-	-		0.2091	0.1650	0.3497	0.7890	0.6269	49.787	62.026
	$\checkmark$	-	$\checkmark$	$\checkmark$	$\checkmark$	$\checkmark$	-	-		0.2011	0.1581	0.3422	0.7902	0.6305	38.776	62.763
	$\checkmark$	-	$\checkmark$	$\checkmark$	$\checkmark$	$\checkmark$	$\checkmark$	-		0.2030	0.1593	0.3403	0.7929	0.6426	<b>37.352</b>	63.052
	$\checkmark$	-	$\checkmark$	$\checkmark$	$\checkmark$	$\checkmark$	$\checkmark$	$\checkmark$		<b>0.1998</b>	<b>0.1556</b>	<b>0.3376</b>	<b>0.7955</b>	<b>0.6441</b>	<b>38.372</b>	<b>63.344</b>

### F. Ablation Study

In this section, we conduct extensive ablation experiments to verify the effectiveness of each module and the loss function we proposed.

1) *Saliency Detection Map  $M$* : As reported in Table IV, we concatenate the saliency detection map  $M$  with input images to provide overall structure prior knowledge. We observe that the SSIM is affected after the utilization of the saliency map since SSIM is more sensitive to texture information. However, as a whole, the performance of the model is improved, especially the FSIM indicators. As displayed in Fig. 1, due to the low quality and lighting variations of the source images, we find that the detected saliency maps have noises and distortions such as the hairs, and faces on the CUFSF dataset. Considering that, we drop the saliency maps and still achieve the **best performance** on the biphasic photo-sketch synthesis results on the CUFSF dataset. Besides, under **normal light conditions**, the saliency detector [21] expresses superior performance on both face photo and sketch<sup>2</sup>, thus leading to the positive impact as shown in Table IV and Fig. 7. Here, as shown in Table V,

<sup>2</sup>There is an open-sourced platform based on this saliency detector for more demos: <http://profu.ai/>

we discard the saliency maps in the following experiments after the injection of semantic layouts.

2) *Parsing Layouts Injection*: Furthermore, we adopt the semantic parsing layouts as two modulation parameters with spatial dimensions injected into the decoder of our network. The semantic layouts aim at providing a kind of spatial supervision of synthesized images. As depicted in Fig. 7 (e) and Fig. 8 (d), the details of the synthesized images are more realistic and vivid in class region. The experiment results also show the effectiveness of parsing layouts injection as shown in Table IV and Table V.

3) *Perceptual Loss and BCE Loss*: In addition, we apply the perceptual loss to improve the high-frequency quality of synthesized images. As displayed in Table IV and Table V, the perceptual loss could significantly reduce the value of FID while increasing FSIM in the face sketch synthesis task. Besides, the Binary Cross-Entropy loss is implemented by BiSeNet [42] to refine the structure layouts of synthesized images. As illustrated in Fig. 7 (g) and Fig. 8 (f), the synthesized human faces retain more distinct facial contours.

4) *Intra-class Semantic Graph Loss*: Moreover, we propose a novel Intra-class semantic Graph (IASG) loss to restrain the

TABLE VI  
ABLATION STUDY OF BIPHASIC ITERATIVE TRAINING STRATEGY.  $\uparrow$  INDICATES THE HIGHER IS BETTER,  $\downarrow$  INDICATES THE LOWER IS BETTER.

		Sketch Synthesis					Photo Synthesis				
Iteration		Initial-0	Iteration-1	Iteration-2	Iteration-3	Iteration-4	Initial-0	Iteration-1	Iteration-2	Iteration-3	Iteration-4
CUFS	LPIPS(alex) $\downarrow$	0.1446	0.1447	<b>0.1406</b>	0.1432	0.1483	0.1571	0.1497	0.1563	<b>0.1497</b>	0.1518
	LPIPS(squeeze) $\downarrow$	0.0995	0.0991	0.0988	<b>0.0986</b>	0.1007	0.1306	0.1237	0.1306	<b>0.1225</b>	0.1248
	LPIPS(vgg-16) $\downarrow$	0.2727	0.2665	0.2650	<b>0.2646</b>	0.2656	0.2588	0.2449	0.2442	<b>0.2367</b>	0.2392
	FSIM $\uparrow$	0.7466	0.7468	0.7482	<b>0.7494</b>	0.7474	0.7892	0.7918	0.7973	<b>0.8001</b>	0.7980
	SSIM $\uparrow$	0.5482	0.5419	0.5472	<b>0.5493</b>	0.5424	0.6627	0.6704	0.6778	<b>0.6822</b>	0.6767
	FID $\downarrow$	33.166	30.640	<b>30.092</b>	33.256	34.490	61.726	55.804	54.303	<b>49.925</b>	51.149
	FVR $\uparrow$	86.648	87.382	87.523	<b>87.542</b>	87.359	78.438	79.922	80.423	<b>81.790</b>	80.249
CUFSF	LPIPS(alex) $\downarrow$	0.1896	0.1883	0.1904	<b>0.1867</b>	0.1912	0.2030	0.2040	0.2038	<b>0.1998</b>	0.2011
	LPIPS(squeeze) $\downarrow$	0.1370	0.1361	0.1351	<b>0.1341</b>	0.1352	0.1593	0.1593	0.1585	<b>0.1556</b>	0.1565
	LPIPS(vgg-16) $\downarrow$	0.3349	0.3372	0.3347	<b>0.3341</b>	0.3377	0.3403	0.3424	0.3419	<b>0.3376</b>	0.3393
	FSIM $\uparrow$	0.7321	0.7323	0.7322	<b>0.7332</b>	0.7330	0.7929	0.7940	0.7941	<b>0.7955</b>	0.7947
	SSIM $\uparrow$	0.4355	0.4371	0.4384	<b>0.4407</b>	0.4375	0.6426	0.6410	0.6430	<b>0.6441</b>	0.6411
	FID $\downarrow$	28.995	28.462	25.690	<b>24.577</b>	26.031	<b>37.352</b>	46.418	43.447	38.372	40.534
	FVR $\uparrow$	87.023	87.099	87.041	<b>87.109</b>	86.980	63.052	63.228	63.191	<b>63.344</b>	62.774

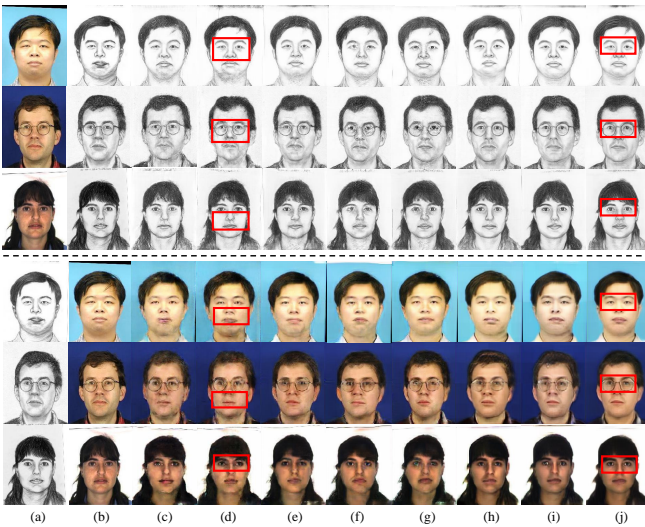


Fig. 7. Ablation studies of synthesized sketches and photos on the CUFS dataset. From top to bottom, the examples are selected from the XM2VTS database, CUHK database, and AR database. (a) Source images, (b) Target Images, (c) Pix2Pix, (d) w/  $M$ , (e) w/  $M + S$ , (f) w/  $M + S$  + Perceptual Loss, (g) w/  $M + S$  + Perceptual Loss + BCE Loss, (h) w/  $M + S$  + Perceptual Loss + BCE Loss + IASG Loss, (i) w/  $M + S$  + Perceptual Loss + BCE Loss + IASG Loss + IRSG Loss, (j) w/  $M + S$  + Perceptual Loss + BCE Loss + IASG Loss + IRSG Loss + ICT Loss. Note that the (h) column represents the results of our preliminary work **SDGAN**.

generated images with ground truth. The IASG loss forces the synthesized images to hold more semantic intra-class knowledge. The details of the sketches and photos we generated are more similar to ground truth, such as the texture of the hair, the contour of the ears, the position of the eyebrows, and the eyes are more consistent as represented in Fig. 7 (h) and Fig. 8 (g). More than that, the IASG Loss raises multiple indicators considerably such as LPIPS (alex, squeeze, vgg) as expressed in Table IV and Table V.

5) *Inter-class Structure Graph Loss*: Combined with the IASG loss we proposed, we bring forward a novel Inter-class structure Graph (IRSG) loss that remarkably enhances the performance of our network. As reflected in Table IV and Table V, the SSIM is increased in whole experiments especially on the sketch synthesis task on the CUFS dataset. The IRSG loss allows the synthesized sketches to become



Fig. 8. Ablation studies of synthesized sketches and photos on the CUFSF dataset. (a) Source images, (b) Target Images, (c) Pix2Pix, (d) w/  $S$ , (e) w/  $S$  + Perceptual Loss, (f) w/  $S$  + Perceptual Loss + BCE Loss, (g) w/  $S$  + Perceptual Loss + BCE Loss + IAG Loss, (h) w/  $S$  + Perceptual Loss + BCE Loss + IASG Loss + IRSG Loss, (i) w/  $S$  + Perceptual Loss + BCE Loss + IASG Loss + IRSG Loss + ICT Loss. Note that the (g) column represents the results of our preliminary work **SDGAN**.

more structure-coordinated. It can be observed that in Fig. 7 (i) and Fig. 8 (h), the sketches are more vivid and distinct.

6) *Iterative Cycle Training Loss*: Eventually, we design a novel biphasic Iterative Cycle Training (ICT) loss to boost the training of sketch and photo synthesis. There are multi-stage iterations in this training strategy. To examine the comprehensive training procedure, we express the results in Table VI. After conducting three times iterations, the network tends to converge and reach its optimum at the third iteration. As depicted in Fig. 7 (j) and Fig. 8 (i), the synthesized sketches and photos contain more personal characteristics. The details of the face images are more meticulous without less blurring and noise such as the eyelashes, hairstyles, and teeth.

#### G. Heterogeneous Face Verification Rate

Meanwhile, we exploit the face verification rate (FVR), deployed by the Face++ API, to report the identity preservation ability of our multi-variation models, as highlighted in Table IV and Table V. Our method synthesizes face photos and sketches from heterogeneous domains. Comprehensively, in the CUFS dataset, the FVR increases distinctly from the back-



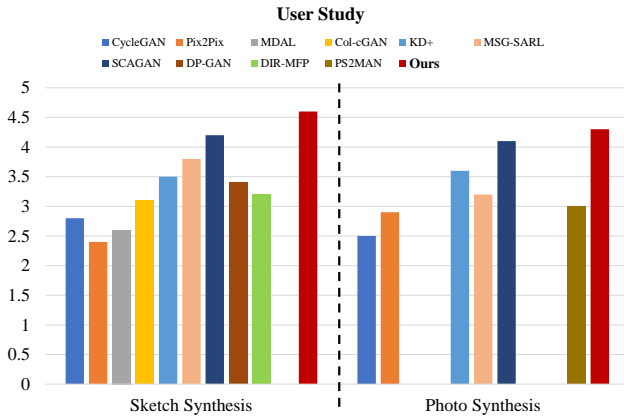


Fig. 9. User study on the sketch synthesis and photo synthesis tasks. There are many approaches that can only achieve the unidirectional sketch synthesis since the photo synthesis task is more challenging.

bone to the final model by 3.332 (84.252→87.542) for sketch synthesis and 8.253 (73.527→81.780) for face photo synthesis. Similarly, the proposed method improves the FVR considerably despite the deformation between the paired sketch photo in the CUFSS dataset. To be more specific, the FVR increases significantly after we exploit the intra-class and inter-class representational graph loss functions, especially in the CUFSS dataset. Although there are deformations between the photos and sketches in the CUFSS dataset, the proposed graph loss functions improve the FVR by 0.511 ( 86.512→87.023) for sketch synthesis and 1.026 (62.026→63.052) for photo synthesis. This highlights the robustness of our proposed graph representation algorithms.

#### H. User Study

We conduct a user study to further analyze the visual quality of the generated biphasic photo-sketch from different methods. In particular, we recruit 20 volunteers and ask them to give feedback scores ranging from 0-5 (the higher, the better) of the generated faces. The evaluation perceptions consist of naturalness and authenticity. The statistical results are reported in Fig. 9. Our method (*i.e.*, the red column) achieves the best performance on both sketch and photo synthesis tasks. This strongly proves our key insight on building the two types representational graphs to model the spatial structure information of human faces.

#### V. CONCLUSION

In this paper, we propose a Semantic-Driven Generative Adversarial Network with Graph Representation Learning for biphasic face photo-sketch synthesis by utilizing saliency detection and face parsing layouts as prior information. In particular, parsing layouts are employed to construct two types of representational graphs that restraint the intra-class and inter-class features of the synthesized images. These graphs could enforce our network to generate the considerate face structure and details. In addition, based on the observation that the paired photo- sketch shared many personal characters, we design a novel biphasic iterative cycle training strategy to

refine the high-frequency quality of the synthesized images. Extension experiments are conducted to verify the effectiveness of proposed each module.

Although the proposed method achieves state-of-the-art performance, there are still limitations in our work. The photos generated in the CUFSS dataset are not vivid and realistic leading to the low face verification rate of the synthesized photos. These issues are caused by the deformation between photos and sketches in the dataset. In addition, in terms of a few indicators, our method is still not optimal implying there are many improvements that can be done. In the future, we will pay more attention to the biphasic face photo-sketch synthesis when facing the large deformations between the paired human photo and sketch.

#### REFERENCES

- [1] X. Wang and X. Tang, "Face photo-sketch synthesis and recognition," *IEEE Trans. Pattern Anal. Mach. Intell.*, vol. 31, no. 11, pp. 1955-1967, 2008.
- [2] N. Wang, D. Tao, X. Gao, X. Li, and J. Li, "A comprehensive survey to face hallucination," *Int. J. Comput. Vis.*, vol. 106, no. 1, pp. 9-30, 2014.
- [3] X. Tang and X. Wang, "Face sketch synthesis and recognition," in *Proc. IEEE/CVF Int. Conf. Comput. Vis. (ICCV)*, Oct. 2003, pp. 687-694.
- [4] M. Zhu and N. Wang, "A simple and fast method for face sketch synthesis," in *Proc. 16th ACM Int. Conf. Int. Multimedia. Comput. Serv. (ICMCS)*, Aug. 2016, pp. 168-171.
- [5] L. Jonathan, E. Shelhamer, and T. Darrell, "Fully convolutional networks for semantic segmentation," in *Proc. IEEE/CVF Conf. Comput. Vis. Pattern Recognit. (CVPR)*, 2015, pp. 3431-3440.
- [6] M. Zhang, N. Wang, Y. Li, and X. Gao, "Deep latent low-rank representation for face sketch synthesis," *IEEE Trans. Neural Netw. Learn. Syst.*, vol. 30, no. 10, pp. 3109-3123, Oct. 2019.
- [7] M. Zhu, N. Wang, X. Gao, and J. Li, "Deep graphical feature learning for face sketch synthesis," in *Proc. 26th Int. Joint Conf. Artif. Intell. (IJCAI)*, Aug. 2017, pp. 3574-3580.
- [8] C. Peng, N. Wang, J. Li, and X. Gao, "Universal Face Photo-Sketch Style Transfer via Multiview Domain Translation," *IEEE Trans. Image Process.*, vol. 29, pp. 8519-8534, Aug. 2020.
- [9] N. Wang, D. Tao, X. Gao, X. Li, and J. Li, "Transductive face sketch-photo synthesis," *IEEE Trans. Neural Netw. Learn. Syst.*, vol. 24, no. 9, pp. 1364-1376, Sept. 2013.
- [10] Q. Liu, X. Tang, H. Jin, H. Lu, and S. Ma, "A nonlinear approach for face sketch synthesis and recognition," in *Proc. IEEE/CVF Conf. Comput. Vis. Pattern Recognit. (CVPR)*, Jun. 2005, pp. 1005-1010.
- [11] S. T. Roweis and L. K. Saul, "Nonlinear dimensionality reduction by locally linear embedding," *science*, vol. 290, no. 5500, pp. 2323-2326, 2000.
- [12] H. Zhou, Z. Kuang, and K. K. Wong, "Markov weight fields for face sketch synthesis," in *Proc. IEEE/CVF Conf. Comput. Vis. Pattern Recognit. (CVPR)*, Jun. 2012, pp. 1091-1097.
- [13] N. Wang, X. Gao, L. Sun, and J. Li, "Bayesian face sketch synthesis," *IEEE Trans. Image Process.*, vol. 26, no. 3, pp. 1264-1274, Jan. 2017.
- [14] I. Goodfellow *et al.*, "Generative adversarial nets," in *Proc. Adv. Neural Inf. Process. Syst. (NeurIPS)*, 2014, pp. 2672-2680.
- [15] L. Zhang, L. Lin, X. Wu, S. Ding, and L. Zhang, "End-to-end photo-sketch generation via fully convolutional representation learning," in *Proc. 5th ACM Int. Conf. Multimedia Retr. (ICMR)*, Jun. 2015, pp. 627-634.
- [16] S. Zhang, R. Ji, J. Hu, X. Lu, and X. Li, "Face sketch synthesis by multidomain adversarial learning," *IEEE Trans. Neural Netw. Learn. Syst.*, vol. 30, no. 5, pp. 1419-1428, May. 2019.
- [17] H. Bi, N. Li, H. Guan, D. Lu, and L. Yang, "A Multi-Scale Conditional Generative Adversarial Network for Face Sketch Synthesis," in *Proc. IEEE Int. Conf. Image Process. (ICIP)*, Sept. 2019, pp. 3876-3880.
- [18] S. Duan, Z. Chen, Q. M. J. Wu, L. Cai, and D. Lu, "Multi-Scale Gradients Self-Attention Residual Learning for Face Photo-Sketch Transformation," *IEEE Trans. Inf. Forensics Security*, vol. 16, pp. 1218-1230, 2021.
- [19] M. Zhu, J. Li, N. Wang, and X. Gao, "Knowledge Distillation for Face Photo-Sketch Synthesis," *IEEE Trans. Neural Netw. Learn. Syst.*, pp. 1-14, Oct. 2020.

- [20] J. Yu, X. Xu, F. Gao, S. Shi, M. Wang, D. Tao, and Q. Huang, "Toward realistic face photo-sketch synthesis via composition-aided GANs," *IEEE Trans Cybern.*, pp. 1-13, Mar. 2020.
- [21] X. Qin, Z. Zhang, C. Huang, M. Dehghan, O. R. Zaiane, and M. Jagersand, "U2-Net: Going deeper with nested U-structure for salient object detection," *Pattern Recognit.*, vol. 106, May. 2020.
- [22] X. Qi, M. Sun, W. Wang, X. Dong, Q. Li, and C. Shan, "Face Sketch Synthesis via Semantic-Driven Generative Adversarial Network," in *Proc. IEEE Int. Joint Conf. Biometrics (IJCB)*, Aug. 2021, pp. 1-8.
- [23] S. Zhang, R. Ji, J. Hu, Y. Gao, and C. W. Lin, "Robust Face Sketch Synthesis via Generative Adversarial Fusion of Priors and Parametric Sigmoid," in *Proc. 27th Int. Joint Conf. Artif. Intell. (IJCAI)*, Jul. 2018, pp. 1163-1169.
- [24] M. Zhang, R. Wang, X. Gao, J. Li, and D. Tao, "Dual-transfer face sketch-photo synthesis," *IEEE Trans. Image Process.*, vol. 28, no. 2, pp. 642-657, Feb. 2019.
- [25] Y. Lin, K. Fu, S. Ling, J. Wang, and P. Cheng., "Toward Identity Preserving Face Synthesis between Sketches and Photos Using Deep Feature Injection," *IEEE Trans Ind. Inform.*, April. 2021.
- [26] P. Isola, J. Y. Zhu, T. Zhou, and A. A. Efros, "Image-to-image translation with conditional adversarial networks," in *Proc. IEEE/CVF Conf. Comput. Vis. Pattern Recognit. (CVPR)*, July. 2017, pp. 1125-1134.
- [27] Y. Qu, Y. Chen, J. Huang, and Y. Xie, "Enhanced pix2pix dehazing network," in *Proc. IEEE/CVF Conf. Comput. Vis. Pattern Recognit. (CVPR)*, Jun. 2019, pp. 8160-8168.
- [28] X. Wang, H. Yan, C. Huo, J. Yu, and C. Pant, "Enhancing Pix2Pix for remote sensing image classification," in *Proc. 24th Int. Conf. Pattern Recognit. (ICPR)*, Aug. 2018, pp. 2332-2336.
- [29] T. C. Wang, M. Y. Liu, J. Y. Zhu, A. Tao, J. Kautz, and B. Catanzaro, "High-resolution image synthesis and semantic manipulation with conditional gans," in *Proc. IEEE/CVF Conf. Comput. Vis. Pattern Recognit. (CVPR)*, Jun. 2018, pp. 8798-8807.
- [30] T. Park, M. Y. Liu, T. C. Wang, and J. Y. Zhu, "Semantic image synthesis with spatially-adaptive normalization," in *Proc. IEEE/CVF Conf. Comput. Vis. Pattern Recognit. (CVPR)*, Jun. 2019, pp. 2337-2346.
- [31] L. A. Gatys, A. S. Ecker, and M. Bethge, "Image style transfer using convolutional neural networks," in *Proc. IEEE/CVF Conf. Comput. Vis. Pattern Recognit. (CVPR)*, Jun. 2016, pp. 2414-2423.
- [32] D. Ulyanov, V. Lebedev, A. Vedaldi, and V. S. Lempitsky, "Texture networks: Feed-forward synthesis of textures and stylized images," in *Proc. 33rd. Int. Conf. Mach. Learn. (ICML)*, Jun. 2016, vol. 1, No. 2, p. 4.
- [33] D. Ulyanov, A. Vedaldi, and V. Lempitsky, "Improved texture networks: Maximizing quality and diversity in feed-forward stylization and texture synthesis," in *Proc. IEEE/CVF Conf. Comput. Vis. Pattern Recognit. (CVPR)*, July. 2017, pp. 6924-6932.
- [34] V. Dumoulin, J. Shlens, and M. Kudlur, "A learned representation for artistic style," 2016, *arXiv:1610.07629*. [Online]. Available: <https://arxiv.org/abs/1610.07629>
- [35] X. Huang and S. Belongie, "Arbitrary style transfer in real-time with adaptive instance normalization," in *Proc. IEEE/CVF Int. Conf. Comput. Vis. (ICCV)*, Oct. 2017, pp. 1501-1510.
- [36] S. Cao, W. Lu, and Q. Xu, "Deep Neural Networks for Learning Graph Representations," in *Proc. 30th AAAI Conf. Artif. Intell.*, vol. 30, no. 1, Feb. 2016.
- [37] B. Perozzi, R. Al-Rfou, and S. Skiena, "Deepwalk: Online learning of social representations," in *Proc. 20th ACM SIGKDD Int. Conf. Knowl. Discovery Data Mining (KDD)*, Aug. 2014, pp. 701-710.
- [38] M. Defferrard, X. Bresson, and P. Van der Gheynst, "Convolutional neural networks on graphs with fast localized spectral filtering," in *Proc. Adv. Neural Inf. Process. Syst. (NeurIPS)*, 2016, pp. 3844-3852.
- [39] M. Li, S. Chen, X. Chen, Y. Zhang, Y. Wang, and Q. Tian, "Action-structural graph convolutional networks for skeleton-based action recognition," in *Proc. IEEE/CVF Conf. Comput. Vis. Pattern Recognit. (CVPR)*, Jun. 2019, pp. 3595-3603.
- [40] M. Ren, Y. Wang, Z. Sun, and T. Tan, "Dynamic graph representation for occlusion handling in biometrics," in *Proc. 34th AAAI Conf. Artif. Intell.*, April. 2020, vol. 34, No. 07, pp. 11940-11947.
- [41] L. Yang, A. Sain, L. Li, Y. Qi, H. Zhang, and Y. Z. Song, "S3Net: Graph Representational Network For Sketch Recognition," in *Proc. IEEE Int. Conf. Multimedia Expo (ICME)*, July. 2020, pp. 1-6.
- [42] C. Yu, J. Wang, C. Peng, C. Gao, G. Yu, and N. Sang, "Bisenet: Bilateral segmentation network for real-time semantic segmentation," in *Proc. Eur. Conf. Comput. Vis. (ECCV)*, Sept. 2018, pp. 325-341.
- [43] K. Simonyan and A. Zisserman, "Very deep convolutional networks for large-scale image recognition," 2014, *arXiv:1409.1556*. [Online]. Available: <https://arxiv.org/abs/1409.1556>.
- [44] A. Paszke et al. "PyTorch: An imperative style, high-performance deep learning library," in *Proc. Adv. Neural Inf. Process. Syst.*, 2019, pp. 8026-8037.
- [45] D. Ulyanov, A. Vedaldi, and V. Lempitsky, "Improved texture networks: Maximizing quality and diversity in feed-forward stylization and texture synthesis," in *Proc. IEEE/CVF Conf. Comput. Vis. Pattern Recognit. (CVPR)*, July. 2017, pp. 6924-6932.
- [46] W. Zhang, X. Wang, and X. Tang, "Coupled information-theoretic encoding for face photo-sketch recognition," in *Proc. IEEE/CVF Conf. Comput. Vis. Pattern Recognit. (CVPR)*, June. 2011, pp. 513-520.
- [47] A. Martinez and R. Benavente, "The AR face database," *Comput. Vis. Center, Barcelona, Spain, CVC Tech. Rep.* 24, 1998.
- [48] K. Messer, J. Matas, J. Kittler, J. Luettin, and G. Maitre, "XM2VTSDB: The extended M2VTS database," in *Proc. Int. Conf. Audio-Video-Based Biometric Person Authentication*, 1999, pp. 72-77.
- [49] N. Wang, X. Gao, and J. Li, "Random sampling for fast face sketch synthesis," *Pattern Recognit.*, vol. 76, pp. 215-227, Apr. 2018.
- [50] L. Zhang, L. Zhang, X. Mou, and D. Zhang, "FSIM: A feature similarity index for image quality assessment," *IEEE Trans. Image Process.*, vol. 20, no. 8, pp. 2378-2386, Aug. 2011.
- [51] Z. Wang, A. C. Bovik, H. R. Sheikh, and E. P. Simoncelli, "Image quality assessment: From error visibility to structural similarity," *IEEE Trans. Image Process.*, vol. 13, no. 4, pp. 600-612, Apr. 2004.
- [52] N. Wang, X. Gao, J. Li, B. Song, and Z. Li, "Evaluation on synthesized face sketches," *Neurocomputing*, vol. 214, pp. 991-1000, Nov. 2016.
- [53] R. Zhang, P. Isola, A. A. Efros, E. Shechtman, and O. Wang, "The unreasonable effectiveness of deep features as a perceptual metric," in *Proc. IEEE/CVF Conf. Comput. Vis. Pattern Recognit. (CVPR)*, Jun. 2018, pp. 586-595.
- [54] F. N. Iandola, S. Han, M. W. Moskewicz, K. Ashraf, W. J. Dally, and K. Keutzer, "SqueezeNet: AlexNet-level accuracy with 50x fewer parameters and < 0.5 MB model size," 2016, *arXiv:1602.07360*. [Online]. Available: <https://arxiv.org/abs/1602.07360>
- [55] A. Krizhevsky, I. Sutskever, and G. E. Hinton, "ImageNet classification with deep convolutional neural networks," in *Proc. Adv. Neural Inf. Process. Syst. (NIPS)*, 2012, pp. 1097-1105.
- [56] M. Lucic, K. Kurach, M. Michalski, S. Gelly, and O. Bousquet, "Are GANs created equal? A large-scale study," 2017, *arXiv:1706.08500*, [Online]. Available: <https://arxiv.org/abs/1711.10337>
- [57] C. Szegedy, V. Vanhoucke, S. Ioffe, J. Shlens, and Z. Wojna, "Rethinking the inception architecture for computer vision," in *Proc. IEEE/CVF Conf. Comput. Vis. Pattern Recognit. (CVPR)*, June. 2016, pp. 2818-2826.
- [58] Megvii Inc. *Face++ Research Toolkit*. Accessed: July. 14, 2021. [Online]. Available: <http://www.faceplusplus.com>
- [59] J. Y. Zhu, T. Park, P. Isola, and A. A. Efros, "Unpaired image-to-image translation using cycle-consistent adversarial networks," *Proc. IEEE/CVF Int. Conf. Comput. Vis. (ICCV)*, Oct. 2017, pp. 2223-2232.
- [60] M. Zhu, N. Wang, X. Gao, J. Li, and Z. Li, "Face photo-sketch synthesis via knowledge transfer," in *Proc. 28th Int. Joint Conf. Artif. Intell. (IJCAI)*, 2019, pp. 1048-1054.
- [61] M. Zhu, J. Li, N. Wang, and X. Gao, "A deep collaborative framework for face photo-sketch synthesis," *IEEE Trans. Neural Netw. Learn. Syst.*, vol. 30, no. 10, pp. 3096-3108, Jan. 2019.
- [62] W. Wan, Y. Yang, and H. J. Lee, "Generative adversarial learning for detail-preserving face sketch synthesis," *Neurocomputing*, vol. 438, pp. 107-121, Jan. 2021.
- [63] D. Zhou, N. Wang, C. Peng, Y. Yu, X. Yang, and X. Gao, "Towards Multi-domain Face Synthesis via Domain-Invariant Representations and Multi-level Feature Parts," *IEEE Transactions on Multimedia.*, July. 2021.
- [64] L. Wang, V. Sindagi, and V. Patel, "High-quality facial photo-sketch synthesis using multi-adversarial networks," in *Proc. 13th IEEE Int. Conf. Autom. Face Gesture Recognit.*, May. 2018, pp. 83-90.
- [65] Y. Wu, O. E. F. Bourahla, X. Li, F. Wu, Q. Tian, and X. Zhou, "Adaptive graph representation learning for video person re-identification," *IEEE Trans. Image Process.*, vol. 29, pp. 8821-8830, 2020.
- [66] Jin, M., Zheng, Y., Li, Y. F., Gong, C., Zhou, C., and Pan, S., "Multi-scale contrastive siamese networks for self-supervised graph representation learning," in *Proc. Int. Joint Conf. Artif. Intell. (IJCAI)*, 2021, pp. 1477-1483.
- [67] M. Sun, J. Wang, J. Liu, J. Li, T. Chen, and Z. Sun, "A Unified Framework for Biphasic Facial Age Translation with Noisy-Semantic Guided Generative Adversarial Networks," *IEEE Trans. Inf. Forensics Security*, vol. 17, pp. 1513-1527, 2022.
- [68] Z. Wang, X. Qi, K. Yuan, and M. Sun, "Self-Supervised Correlation Mining Network for Person Image Generation," in *Proc. IEEE/CVF Conf. Comput. Vis. Pattern Recognit. (CVPR)*, June. 2022, pp. 7703-7712.